

Measuring bedload motion time at sub-second resolution using Benford's law on acoustic data

Ci-Jian Yang¹, Jens Martin Turowski², Qi Zhou (Chow)³, Ron Nativ⁴, Hui Tang⁵, and Wen-Sheng Chen⁶

¹National Taiwan University

²GFZ German Research Centre for Geosciences, Potsdam

³Helmholtz Centre Potsdam GFZ German Research Centre for Geosciences

⁴Ben-Gurion University of the Negev

⁵German Research Centre for Geosciences (GFZ)

⁶Center for General Education, National Dong Hwa University

November 8, 2023

Abstract

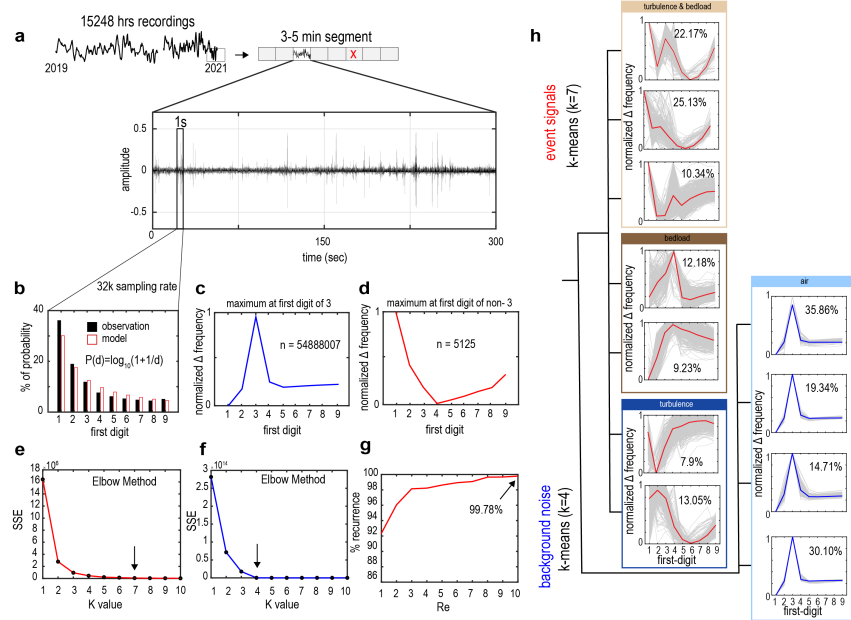
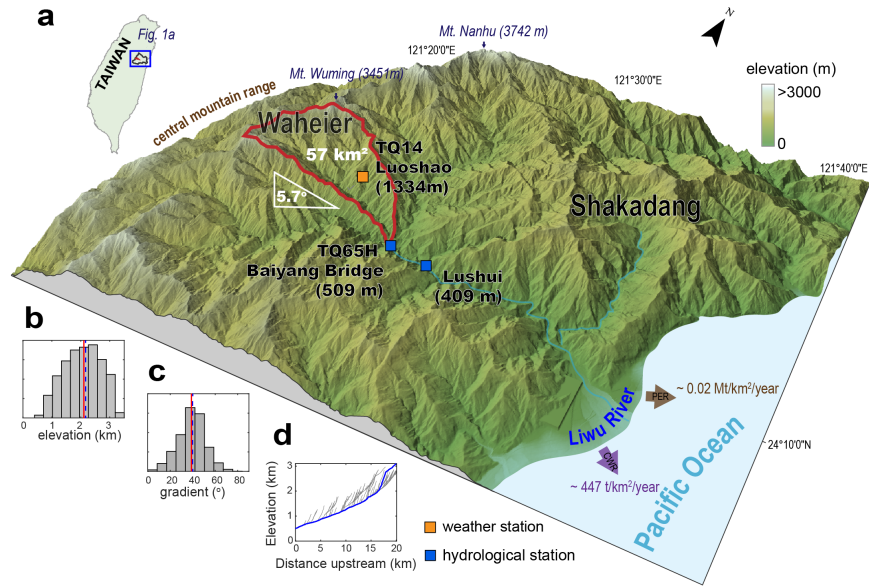
An important component of quantifying bedload transport flux is the identification of the onset of bedload motion. Bedload transport can be monitored with high temporal resolution using passive acoustic methods, e.g., hydrophones. Yet, an efficient method for identifying the onset of bedload transport from long-term continuous acoustic data is still lacking. Benford's Law defines a probability distribution of the first-digit of datasets and has been used to identify anomalies. We apply Benford's Law to the three years of acoustic recordings from a stationary hydrophone in the Taroko National Park, Taiwan. Our workflow allows for monitoring bedload motion in near-real-time, and it is convenient for others to reference. Two bedload transport events were identified during the examined period, lasting 17 and 45 hours, accounting for approximately 0.35% of the time per year.

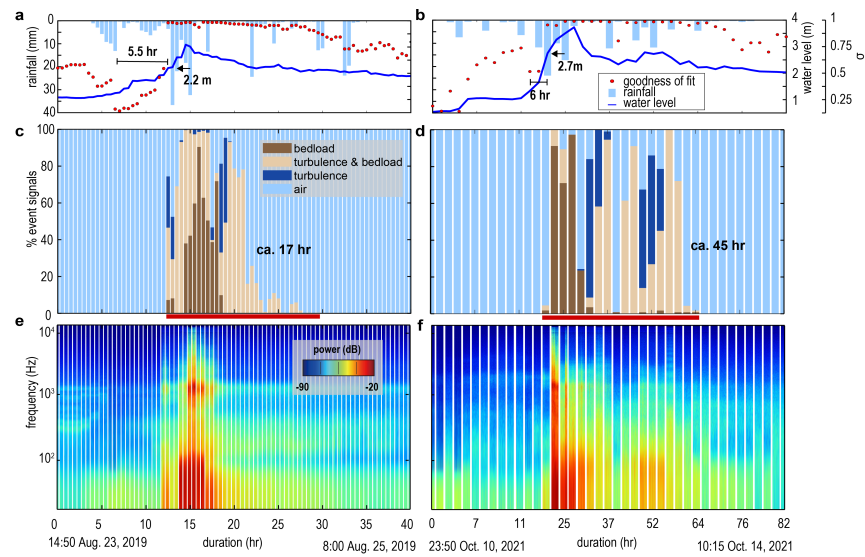
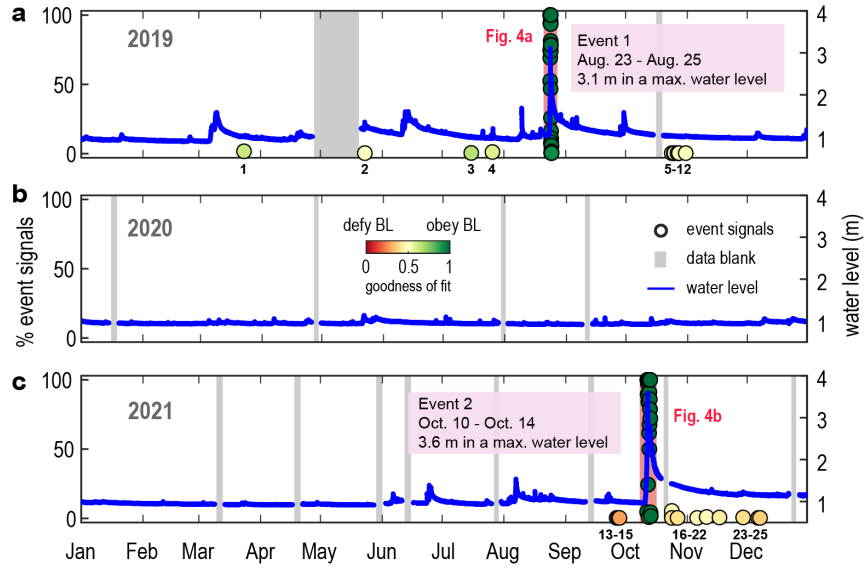
Hosted file

978252_0_art_file_11546629_s3ktx9.docx available at <https://authorea.com/users/696767/articles/685116-measuring-bedload-motion-time-at-sub-second-resolution-using-benford-s-law-on-acoustic-data>

Hosted file

978252_0_supp_11546630_s3rzrc.docx available at <https://authorea.com/users/696767/articles/685116-measuring-bedload-motion-time-at-sub-second-resolution-using-benford-s-law-on-acoustic-data>





1 Measuring bedload motion time at sub-second resolution using 2 Benford's law on acoustic data

3
4 Ci-Jian Yang^{1*}, Jens M. Turowski², Qi Zhou^{2,3}, Ron Nativ^{2,3,4}, Hui Tang², Wen-Sheng
5 Chen⁵

6 ¹Department of Geography, National Taiwan University, Taipei

7 ²Helmholtzzentrum Potsdam, GFZ German Research Center for Geosciences, Potsdam

8 ³Institute of Geosciences, University of Potsdam, Potsdam

9 ⁴Department of Earth and Environmental Sciences, Ben-Gurion University of the
10 Negev, Be'er Sheva

11 ⁵Center for General Education, National Dong Hwa University, Hualien

12 *Corresponding author: Ci-Jian Yang (cijianyang@ntu.edu.tw, No. 1, Sec. 4, Roosevelt
13 Road, Taipei, 10617 Taiwan)

14 Key points:

- 15 ● Long-term, high-frequency acoustic monitoring constitutes huge-volume datasets
16 and an extremely small signal-to-noise ratio.
- 17 ● The distinct first-digit distribution between signal and noise can used to filter out
18 99% of background noise from acoustic recordings.
- 19 ● We tested the method for three year long acoustic data set in Baiyang, two
20 identified bedload transportation events.

21 Abstract

22 An important component of quantifying bedload transport flux is the identification of
23 the onset of bedload motion. Bedload transport can be monitored with high temporal
24 resolution using passive acoustic methods, e.g., hydrophones. Yet, an efficient method
25 for identifying the onset of bedload transport from long-term continuous acoustic data
26 is still lacking. Benford's Law defines a probability distribution of the first-digit of
27 datasets and has been used to identify anomalies. We apply Benford's Law to the three
28 years of acoustic recordings from a stationary hydrophone in the Taroko National
29 Park, Taiwan. Our workflow allows for monitoring bedload motion in near-real-time,
30 and it is convenient for others to reference. Two bedload transport events were

31 identified during the examined period, lasting 17 and 45 hours, accounting for
32 approximately 0.35% of the time per year.

33 **Plain Language Summary**

34 Long-term, high-frequency monitoring of Earth surface processes brings huge
35 datasets and an extremely small signal-to-noise ratio. Benford's Law defines the
36 specific probability distribution of the first-digit of datasets and has been used to
37 identify anomalies and high-energy events. We provide a workflow of applying
38 Benford's Law to identify the onset of the motion of coarse sediment along the river
39 bed at a time resolution of seconds. We identified three separate sound classes in the
40 data related to the noise produced by the motion of pebbles, water flow, and air. The
41 workflow could be referred for other different catchments, events, or datasets. Due to
42 the influence of instrument and background noise on the regularity of the residuals of
43 the first-digit, We recommend identifying the first-digit distribution of the background
44 noise and ruling it out before implementing this workflow.

45 **Keywords** acoustic monitoring, bedload, first-digit, event indicator, early warning
46 system

47

48 **1. Introduction**

49 Bedload transport driven by floods is one of the manifestations of natural processes
50 that strongly affect the Earth's surface system. Bedload transport is a fundamental
51 process in river corridors, with implications for channel stability (e.g. Turowski et al.,
52 2009; Recking et al., 2016), sediment budgets (e.g., Theule et al., 2012), pollution
53 transport (e.g., Stott et al., 2001), fluvial erosion (e.g., Turowski et al., 2008), and
54 aquatic habitats (e.g., Snyder et al., 2009). Bedload transport increases river lateral
55 migration or erosion and deposition, with potentially hazardous effects on
56 downstream residents' lives and property (e.g., Krapesch et al., 2011, Bufe et al.,
57 2019). In Switzerland, bedload transport caused cumulative financial losses of USD

58 5.3 billion from 1972 to 2011, about one-third of the total natural hazard damage
59 during that period (Badoux et al., 2014). Reliable approaches for bedload monitoring
60 are needed not only for hazard warning systems but also for quantifying fluvial
61 processes.

62 Monitoring in extreme environments during storms can complement existing
63 observations of fluvial processes, such as understanding temporal changes in bedload
64 motion and calculating the proportion of total sediment flux. Yet, the estimations of
65 bedload transport from long-term monitoring systems are limited. Passive acoustic
66 methods, e.g., hydrophones, and seismometers, are sensitive to bedload motion (e.g.,
67 Geay et al., 2017; Burtin et al., 2016) and able to obtain the data at a safe distance.
68 Acoustic data from hydrophones, where bedload impacts can be heard directly,
69 provide a benchmark that is not usually available when using seismic data only (e.g.,
70 Roth et al., 2017). In addition, high-frequency acoustic monitoring allows for
71 detecting bedload motion in realtime, which could be used for warning systems,
72 improving over generic empirical values calibrated on previous events (Abancó et al.,
73 2012; Baum & Godt, 2010; Badoux et al., 2014; Marra et al., 2016). However, an
74 automatic and efficient method for constraining the onset of bedload transport events
75 from long-term acoustic data is still lacking.

76 Benford's Law defines a specific probability distribution of the first-digit of datasets.
77 It predicts that a first-digit of one occurs about 30% of the time in a given dataset,
78 three times higher than the value of 1/9 expected from a uniform distribution.
79 Benford's Law has been used to identify fraud in accounting or political votes (Nigrini,
80 1999). It appears in natural data as well. For example, nearly half of a million US
81 annual average flows and the size of global lakes and wetlands follow Benford's Law
82 (Nigrini and Steven, 2007). Benford's Law has also been used to distinguish noise
83 from chaotic processes when the process causes higher energy events than baseline

84 noise (Li et al., 2015). For example, the onset of earthquakes has been identified using
85 Benford's Law on seismic amplitude data (Sambridge et al., 2010; Díaz et al., 2015).
86 In addition, accurate and complete observational data on the traveled distance of
87 tropical cyclones conform to Benford's Law. Thus, Benford's Law residuals become a
88 tool for evaluating data quality and homogeneity (Joannes-Boyau et al., 2015).
89 In underwater acoustic recordings, the median power of bedload-generated noise in
90 the frequency range between 10^3 Hz and 10^4 Hz is about 2.5 orders of magnitude
91 higher than that of the low flow period at the same reach (Geay et al., 2017).
92 Therefore, we hypothesize that the change in the first-digit distribution of acoustic
93 amplitudes can properly identify high-energy events, and in principle, we expect that
94 the first-digit distribution has the potential to be an indicator that can be used to
95 separate sound categories, i.e., air, waterflow, and motion of pebbles. For example, the
96 95th percentile of power spectral density ranges from 10^4 to 5×10^4 (Geay et al., 2017).
97 This half-order of magnitude data range results in a new first-digit distribution
98 different from Benford's Law.
99 Here, we develop a simple statistical tool based on mathematical law that can
100 automatically and efficiently identify bedload signals from long-term acoustic
101 recordings. We apply the method to three years of underwater audio observations at
102 Baiyang hydrometric station. We demonstrate the potential of Benford's Law in
103 distinguishing sound categories, which we propose is significant for improving
104 bedload flux calculations.

105

106 **2. Materials and Methods**

107 **2.1 Benford's Law**

108 Benford's Law (Benford, 1938) states that the probability of the first-digit is
109 non-uniform but rather obeys Eq. (1):

110
$$P_D = \log_{10}(1 + 1/D). \quad (1)$$

111 Here, P_D is the probability of the first-digit D occurring ($D = 1, \dots, 9$). For example,
112 the first-digit of -0.01, 1, or 1e8 are all 1. The law suggests that numbers beginning
113 with a one occur about 30.1% of the time in some natural datasets, while those with
114 the first- digit of two occur about 17.6% of the time, and so on, down to the first-digit
115 of nine occurring about 4.6% of the time.

116 We use a least-squares misfit measure to quantify the discrepancy between the
117 observed and theoretical probability of the first-digit (Joannes-Boyou, 2015). We
118 subtract the misfit from one and define it as the goodness of fit (2):

119
$$\sigma = 1 - \sum_{(D=1)}^9 \left(100 \frac{n_D}{n} - P_D\right)^2, \quad (2)$$

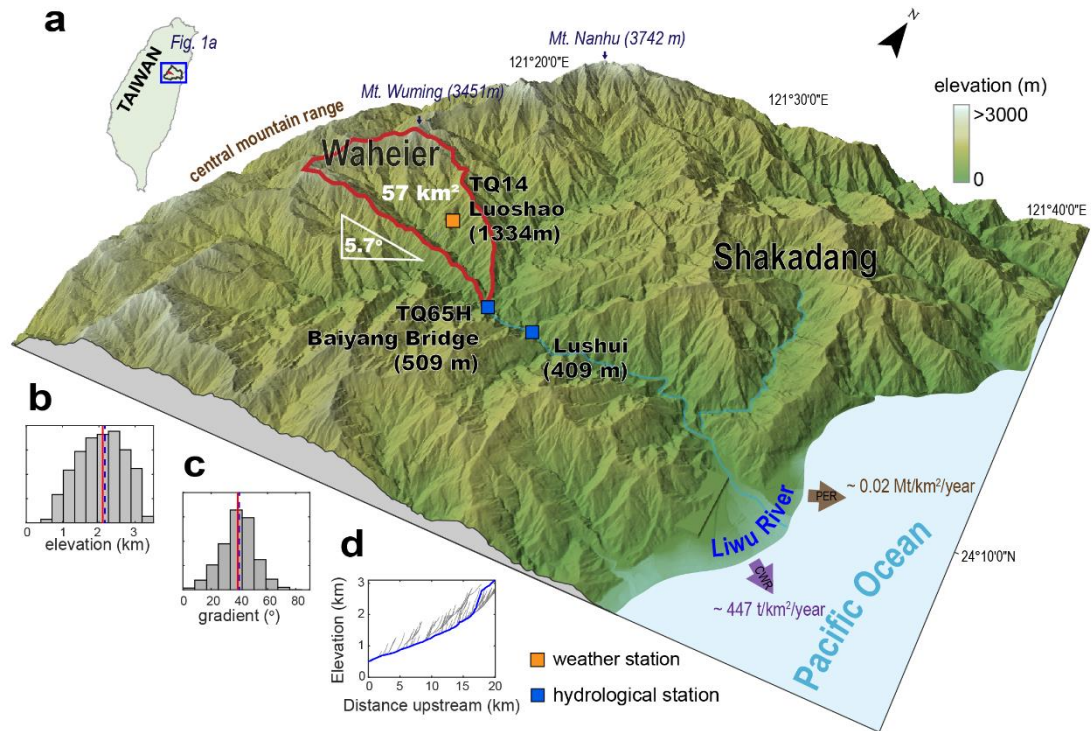
120 where P_D is the theoretical probability of data with the first-digit D as given by
121 Benford's Law, n_D is the number of data with the first-digit D , and n is the total
122 number of data. The first-digit distribution can be independently assessed for the
123 goodness of fit against theoretical values of Benford's Law, eliminating the need for
124 other detecting methods, such as short-time average/long-time average (STA/LTA),
125 which require long-term observations. In addition, we calculate the acoustic amplitude
126 difference between the 75th and 25th percentile (interquartile range) for every second
127 as an index of the data range.

128 **2.2 Study site and monitoring**

129 The Liwu catchment is located in eastern Taiwan (Figure 1a), experiencing
130 high-frequency seismic activity and rapid tectonic uplift of 5.5 mm yr⁻¹ (Petley et al.,
131 1997). The mean annual rainfall is about 2.5 m, and typhoons are the dominant source
132 of heavy rainfall, accounting for 66% of the annual discharge (Huang et al., 2012).
133 This results in 20,000 t km⁻² y⁻¹ of physical denudation rate calculated from suspended
134 sediment (Dadson et al., 2003) and 18 t km⁻² y⁻¹ derived from silicate weathering,

135 which is one of highest measured so far in the world for felsic lithologies (Calmels et
136 al, 2011). The Liwu provides a natural laboratory with active driving forces, relatively
137 minor human influence, and a unique opportunity to investigate bedload dynamics
138 from a typhoon-dominated system.

139 Baiyang hydrometric station is located on the outlet of Waheier catchment, a tributary
140 of Liwu River, which drains 57 km². Elevation in the Waheier catchment spans from
141 509 to 3451 m with a mean of 2055 m (Figure 1b). The mean hillslope gradient is
142 39.5° (Figure 1c), and the mean channel gradient is about 5.7%. The length of the
143 mainstream is 20.8 km (Figure 1d). Baiyang hydrometric station was installed at
144 Baiyang Bridge in April 2018. There, underwater acoustic noise has been
145 continuously measured at a 32 kHz sampling rate using a broadband hydrophone,
146 Aquarian H2a-XLR (Aquarian Audio, 2013). The hydrophone is protected by a 30 cm
147 metal tube attached to the bedrock close to the water surface at a low flow of about ~1
148 m. Five-minute-resolution measurement of the water stage is measured using a Radar
149 Level Sensor (RLS) with an accuracy of 10 mm. Half-hour time-lapse imagery is
150 recorded by three D30 Canon cameras with different viewpoints. Within the same
151 catchment, Luoshao station (Figure 1) provides minute-resolution rainfall
152 measurements using an automatic weather station, WXT-536.



153

154 **Figure 1.** (a) Topographical 3D view of the Liwu catchment and the study site. In the
 155 outlet of the Waherier catchment, Baiyang hydrometric station (TQ65H) monitors
 156 river acoustic sounds and provides hydrometric data. Minute-resolution rainfall is
 157 obtained from the Luoshao (TQ14) weather station. (b) Histogram of elevation of
 158 Waheier catchment, red line denotes median value, and blue dash denotes mean value.
 159 (c) Histogram of hillslope gradient of Waheier catchment, red line denotes median
 160 value, and blue dash denotes mean value. (d) Longitudinal profile of the upstream
 161 from the Baiyang station

162 2.3 Data preparation and audio recording visualization

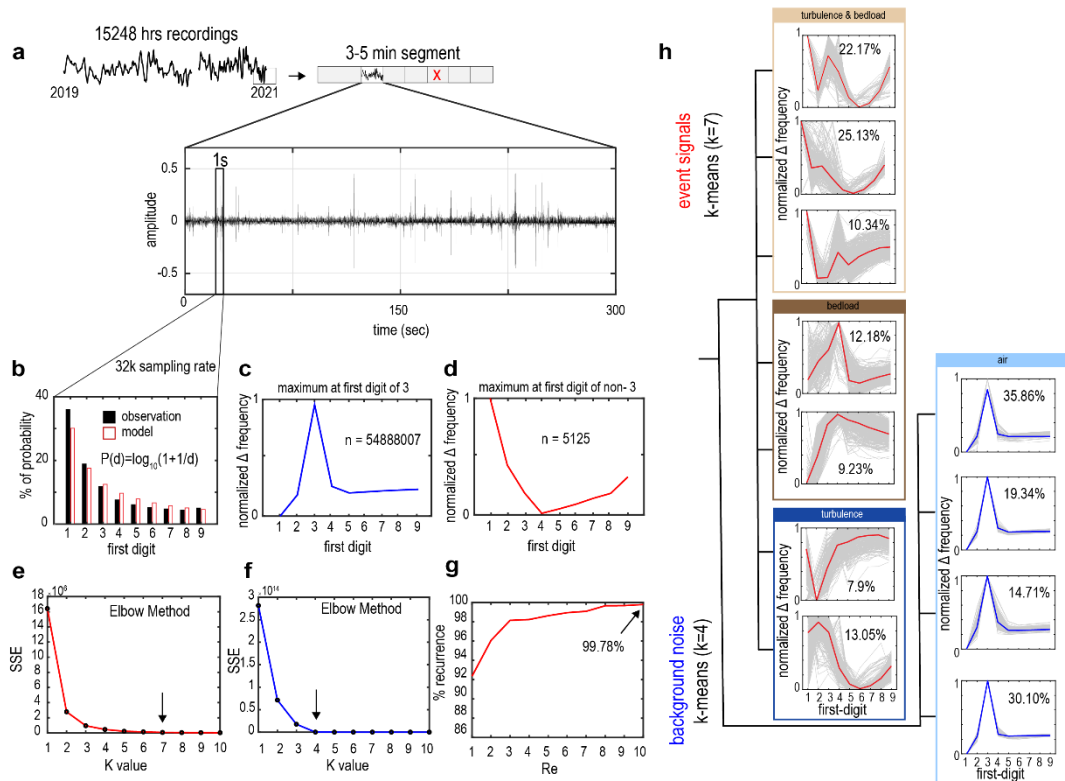
163 Signal processing, including detrending and deconvolution, may result in changes in
 164 acoustic amplitude, which may mask Benford's Law. Therefore, we did not
 165 pre-process the audio data. This has the further advantage of significantly reducing
 166 the computational cost of our method. Here, we used the acoustic recordings from the
 167 stationary hydrophone deployed from 2019 to 2022 (Figure 2a). The audio data was
 168 split into .mp3 files of three to five minutes in length. After removing damaged and
 169 short-period files (< 1 minute), we obtained a total of 15,248 hours of acoustic
 170 recordings. Each second of recording has 32,000 individual acoustic amplitude
 171 measurements, sufficient to calculate the probability distribution of the first-digit. To

172 visualize audio recordings, we transformed the signals from the time domain to the
 173 frequency domain using a short-time Fourier transform to obtain the power spectral
 174 density.

175 2.4 Sound classification via residual probability distribution

176 To distinguish between different sound categories based on the probability of
 177 first-digit, our workflow contains three steps. First, we calculate the residual between
 178 the probability of first-digit for observed data and Benford's theoretical frequencies,
 179 and we categorize the residuals into two groups: event signals and background signals.
 180 Second, , we identify sound categories using the k-means clustering and determine the
 181 number of clusters using the Elbow method, along with the method to assess the
 182 clustering stability. Third, we calculate the time-series ratio of respective sound
 183 categories. These steps are described in detail in the supplementary.

184



185

186 **Figure 2.** Workflow of the applied Benford's law to sound combinations. (a)

187 Schematic diagram of the acoustic amplitude along the entire study period. An
188 acoustic data file (*.mp3) is generated for every 3 to 5 minutes of acoustic recordings.
189 (b) A comparison of the probability distribution of Benford's Law model and
190 observation in %, P is the probability, and D is the first-digit. (c) Schematic diagram
191 of the category of normalized probability difference that maximum is not the
192 first-digit with three. (d) The category of normalized probability difference that
193 maximum is the first-digit with three. (e) Determining the k-value (number of clusters)
194 of event noise according to the Elbow method. (f) Determining the k-value of
195 background noise with the Elbow method. (g) Determining the parameter Re (number
196 of times to repeat clustering). (h) Categories of normalized probability difference
197 distribution, classified by the k-means method. Percentages represent proportions in
198 the same group.

199 **3. Results**

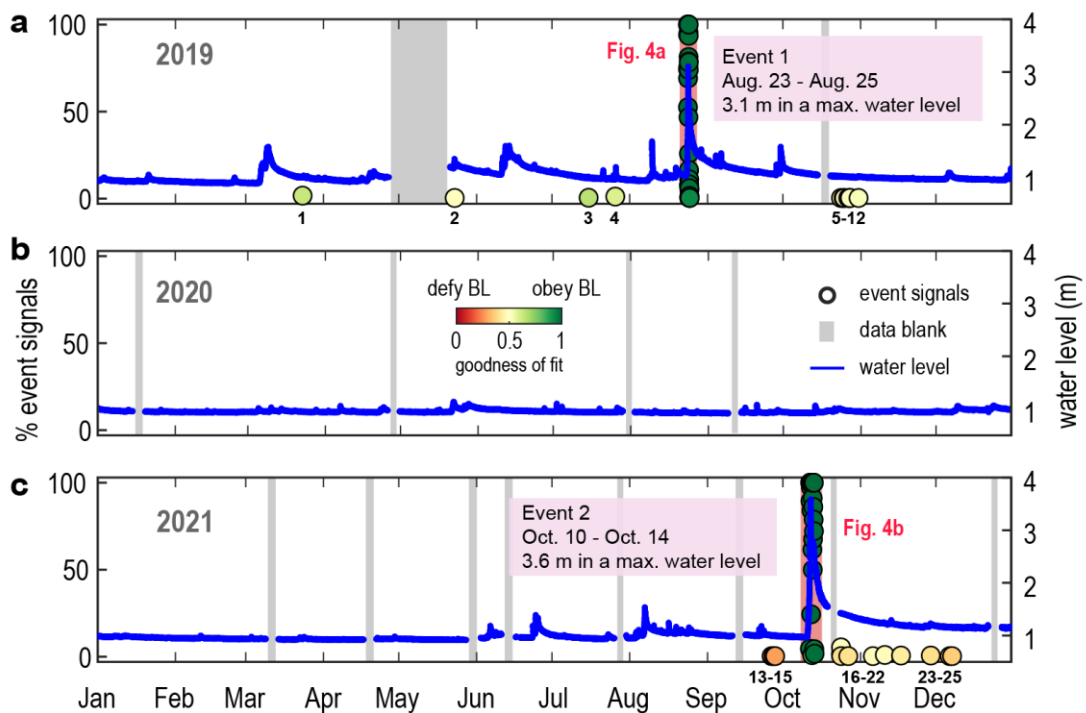
200 **3.1 Sound classification determined by k-means clustering**

201 Our results from k-means clustering show seven classes for event signals (n=5125)
202 and four classes for background noise (n=54888007). The Elbow method provides the
203 k value to satisfy the statistical objective of minimizing within-cluster error in the
204 k-means method, and it may lead to overfitting, surpassing the requirements for sound
205 identification. For example, background noise can be separated into four classes, but
206 they do not hold physical meaning. We found distinctive characteristics in the residual
207 probability, where specific types of sounds exhibit the same largest residual position.
208 For example, the largest residual value at the first-digit with a three is always an air
209 sound; the largest residual value at the first-digit with a one is mainly the sound of
210 turbulence with sediment impacts, which occurs about 57.6% of the total event signal;
211 the largest residual value at the first-digit with a four is mainly the sound of sediment
212 impacts that are inferred to be bedload transport, occurring at 21.41% of the total
213 event signal. The other two classes accounted for 20.95% in total, mostly the sound of
214 turbulence. Notably, the largest residuals of turbulence are not in the same position.
215 To simplify the acoustic diversity, we merged them according to the location of the
216 largest residual value into four classes of sounds, i.e., bedload motion, turbulence with

217 bedload motion, turbulence, and air (Figure 2h).

218 **3.2 The goodness of fit marks bedload transportation events**

219 From 2019 to 2021, two bedload transport events occurred at Baiyang station. The
220 first event happened on Aug. 24, 2019, with a maximum water level of 3.1 m. The
221 goodness of fit is nearly one during this period, meaning that the first-digit
222 distribution closely follows Bedford's law, and the ratio of event signal increases to
223 100% (Figure 3a). The second event happened on Oct. 10, 2021, with a maximum
224 water level of 3.6 m. Similarly, the goodness of fit is nearly one during this period,
225 and the ratio of event signal increases to 100% (Figure 3c). In 2020, the water level
226 did not exceed 1.1 m, and bedload transport was negligible (Figure 3b). Apart from
227 these two events, 25 audio files contain event signals, accounting for 28 seconds, 0.54
228 % of the total event signal. In addition, the mean amplitude difference ($75^{\text{th}} - 25^{\text{th}}$) of
229 these 25 audio files is $0.007 \pm 3 \times 10^{-5}$, and the mean power calculated from the
230 spectrogram is -85.21 ± 6.14 (Table S1). Given low values in duration, acoustic
231 intensities, the goodness of fit, and the ratio of event signal, we ruled out these 25
232 audio recordings from bedload transport events.



233

234 **Figure 3.** Three-year time series of event signal ratios, the goodness of fit, and river
 235 water levels. (a–c) represents the years from 2019 to 2021. Blue lines are water
 236 hydrographs, and circles denote event signals in %, colored by the goodness of fit.
 237 Numbers beside the circles mark the misidentified 25 audio files.

238

239 3.3 Changes in residual probability of the first-digit distribution during the two 240 events

241 Our examination demonstrates that the hydrophone captures sounds emanating from
 242 various physical mediums, including air, water flow, and bedload motion throughout
 243 the monitoring period. In the first event, the ratio of bedload motion occurrence
 244 increased from 7.3% at 04:50 on Aug. 24, 2019, with a critical stage of 2.2 m to
 245 90.1% after 3 hours, followed by a decrease to 9.9% at 10:50 on Aug. 24, about 6
 246 hours later. Sounds of turbulence with sediment impact start with bedload motion but
 247 dominate the source of sound in the early and late stages of the event by over 52% of
 248 the five-minute sound contribution. Sounds reflecting sediment impact account for
 249 82.5% of five-minute sound contribution during the peak of bedload motion.
 250 Eventually, the bedload motion ends at 21:50 on Aug. 24, while the dominant sound

251 contributor becomes air (background noise) (Figure 4c).
252 During the second event, the ratio of bedload motion in five-minute sound
253 contribution increased from 1.8% at 18:55 on Oct. 11, 2021, with a critical stage of
254 1.9 m, to 97.4% at 03:55 on Oct. 12 with a critical stage of 2.7 m. Contrary to the first
255 event, the ratio of bedload motion lasted until 15:55, the end of the event on Oct. 13.
256 At the time of the local low water stage of 2.4 m, bedload motion was halted. Then,
257 the motion was re-activated at a higher water level of 2.5 m with the 1% ratio of
258 bedload motion. Similarly, the occurrence of turbulence together with bedload
259 transport dominates the sound source in the recession limb by over 60%. By 15:55 on
260 Oct. 12, the sound is fully generated by air (Figure 4d). Based on the occurrence and
261 end time of bedload signals, we calculate the duration of the two bedload transport
262 events, yielding 17 and 45 hours, respectively, constituting roughly 0.35% of the time
263 per year, which is equal to 30.7 hours/year.

264 **4. Discussion**

265 **4.1 Applications of the acoustic and statistical method**

266 We present an automatic and efficient workflow to identify the onset of bedload
267 transport and reveal the dynamic sound combinations during sediment transport
268 events. We have also proposed recommendations regarding data processing. The
269 distribution of the first-digit in background noise may vary depending on the static
270 voltage of the instrument, e.g., loggers, seismic or acoustic stations, and the type of
271 noise. We propose visualizing short-term audio files and applying Benford's Law to
272 establish a connection between background noise and the distribution of first-digit,
273 which significantly reduced computational expenses.

274 The residual probability of bedload signals always appears at the location of the
275 first-digit with four in this study, which may vary depending on the monitoring
276 instrument, but can be verified through human listening and acoustic spectrograms.

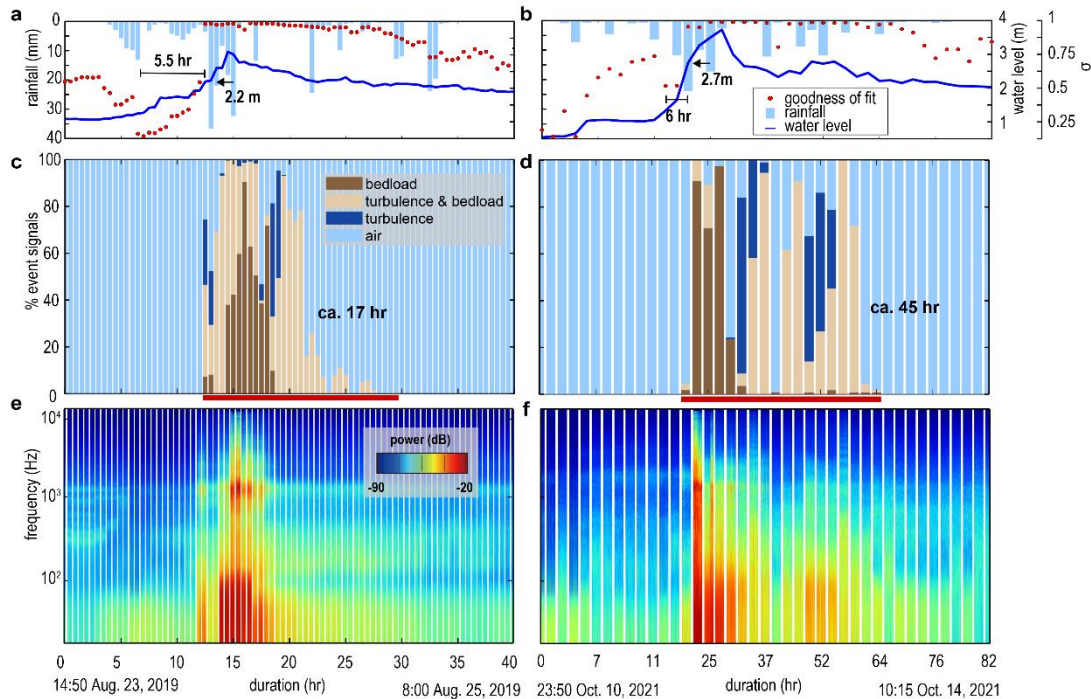
277 Therefore, we recommend conducting short-term validations between the residual
278 probability and the sound types. Although k-means clustering offers the advantage of
279 fast computation, we encountered the issue of overfitting. we have merged 11 types of
280 sounds into 4 types based on human listening. We recommend using supervised
281 classification tools for distinguishing different sounds.

282 **4.2 The sound combination determined by residual probability reflects bedload** 283 **dynamics**

284 Using the residual probability of the first-digit distribution, we classify sounds at a
285 second timescale and accurately determine the timing and critical state for the onset of
286 bedload motion. Sound combinations reflect dynamic flooding events where
287 numerous processes may occur individually or concurrently (e.g., Fig. 4). Moreover,
288 the critical state of the second event is 1.24 times higher than the first event. We infer
289 that following the bedload transport event, the bed morphology was altered, As such,
290 gravels inlaid with each other, forming higher critical shear stress for the onset of
291 bedload motion (Turowski et al., 2011). In addition, the study in Erlenbach torrent
292 shows that small to intermediate past flows contribute to the development of channel
293 stability and high-magnitude flows decrease the critical shear stress (Masteller et al.,
294 2019).

295 The ratio of bedload sound temporally coincides with the mean of the acoustic power
296 calculated from the spectrogram (Figure S2). The spectrogram at Baiyang station on
297 Aug. 23 to 25, 2019 (Figure 4e) shows that before the onset of the bedload motion
298 (defined by the goodness of fit; Figure 4a), the acoustic power below 100 Hz is about
299 two orders of magnitude higher than in other frequency bands, which can be attributed
300 to the sound of flowing water. When the bedload transport begins, the acoustic power
301 at frequency bands of ~1000 Hz increases by about five orders of magnitude. This
302 increase lasts for about six to seven hours. The October 2021 spectrogram (Figure 4f)

303 exhibits a similar pattern; the acoustic power increases by several orders of magnitude
 304 at high frequency. When the ratio of bedload sound decreases, the acoustic power also
 305 decreases.



306
 307 **Figure. 4** Sound combinations of the two bedload transportation events. (a–b)
 308 Rainfall, water level, and goodness of fit. Periods denote the duration of the decline
 309 period in goodness of fit. (c–d) Time series of sound combinations. Colors represent
 310 the source of the sound (see legend). (e–f) Semilogarithmic spectrograms of acoustic
 311 signals.

312 4.3 Decreasing goodness of fit at incipient flooding

313 The goodness of fit not only identifies the onset of bedload transport but also has the
 314 potential to recognize changes in hydraulics. We found that decreasing goodness of fit
 315 and increasing water level are abrupt at incipient flooding (Figure 4a–4b). In the first
 316 event, 5.5 hours before the onset of bedload motion, the goodness of fit decreased
 317 from 0.63 to 0.45, and the water level increased conversely from 1.19 to 1.24 m. In
 318 the second event, 6 hours before bedload motion, the goodness of fit decreases from
 319 0.79 to 0.63, and the water level increases conversely from 1.5 m to 1.7 m.

320 We found sound sources with sound durations shorter than one second which we

321 consider as pulse-type sources (Figures S1a–S1b). The pulses may be caused by
322 advancing flooding, where the surging water surface entrains a large number of air
323 bubbles, making the hydrophone susceptible to a mechanical pulse sound. The sound
324 increases amplitude by less than an order of magnitude, prohibiting the full
325 application of Benford's Law and reducing the goodness of fit. Even though such
326 pulse-type sound is defined as background noise in this study, it combines with the
327 change in the goodness of fit, we could grasp this hydrological change. If such an
328 abrupt decrease in the goodness of fit at the rising limb of the hydrograph is consistent
329 throughout various study sites, it may constitute an important feature that can be
330 utilized to improve early warning systems for Earth surface flows, including bedload
331 transport and debris flows.

332 **5. Conclusion**

333 A method that can rapidly and accurately detect the onset of bedload transport in
334 real-time is crucial for disaster warnings and calculating sediment flux. We use the
335 probability change in first-digit distribution from the two bedload transport events to
336 establish a workflow flow of event detection and sound classification. With our
337 workflow, we were able to filter out >99% of the background noise from acoustic
338 recordings and focus on flooding event acoustic signals that can further be separated
339 into three sound classes by statistical clustering tools. We propose a statistical
340 ‘goodness of fit’ between the theoretical Benford’s Law and empirical data and find
341 this parameter to match the onset of bedload motion. Hence, we propose that the
342 operating timing of an expensive monitoring tool, e.g., an automatic river water
343 sampler, can be initiated using this simple parameter.

344 Given that Benford's Law has demonstrated usefulness in acoustic amplitude analysis,
345 and that Environmental Seismology has been widely used in monitoring fluvial
346 processes (e.g., Burtin et al., 2016; Cook et al., 2021; Dietze et al., 2019, 2022; Walter

347 et al., 2017). Therefore, we suggest that applying environmental seismology in
348 parallel with Benford's Law can be useful in identifying anomalous events in any kind
349 of real-time data series. We used the audio data at a sampling rate of 32 kHz, which is
350 sufficient for Benford's Law calculation. Increasing the time resolution to sub-second
351 resolutions is possible. However, since the common sampling rate of the
352 seismometers is 200 Hz, which covers most environmental processes, reducing the
353 time resolution to the minute scale is necessary to acquire a dataset with an adequate
354 sample size and expected data range. Nonetheless, minute-scale observations are
355 sufficient for early warning of fluvial disasters.

356 **Data Availability Statement**

357 All data and MATLAB code analyzed in this study are available at
358 <https://doi.org/10.6084/m9.figshare.24493273.v1>.

359

360 **References**

- 361 Abancó, C., Hürlimann, M., Fritschi, B., Graf, C., and Moya, J. (2012).
362 Transformation of ground vibration signal for debris flow monitoring and
363 detection in alarm systems. *Sensors*, 12(4), 4870–4891.
- 364 Aquarian Audio (2013) Aquarian Audio Products H1a Hydrophone User's Guide:
365 Anacortes, Wash. Aquarian Audio Products. [https://www.aquarianaudio.com/
366 AqAudDocs/H1a_manual.pdf](https://www.aquarianaudio.com/AqAudDocs/H1a_manual.pdf).
- 367 Badoux, A., Andres, N., Turowski, J. M. (2014). Damage costs due to bedload
368 transport processes in Switzerland. *Nat.Hazards Earth Syst. Sci.*, 14, 279–294,
369 <https://doi:10.5194/nhess-14-279-2014>
- 370 Baum, R. L., & Godt, J. W. (2010). Early warning of rainfall-induced shallow
371 landslides and debris flows in the USA. *Landslides*, 7(3), 259–272.
372 <https://doi.org/10.1007/s10346-009-0177-0>

373 Benford, F. (1938). The Law of Anomalous Numbers. *Proceedings of the American*
374 *Philosophical Society*, 78(4), 551–572. <http://www.jstor.org/stable/984802>

375 Bufe, A., Turowski, J. M., Burbank, D. W., Paola, C., Wickert, A. D., and Tofelde,
376 S. (2019). Controls on the lateral channel-migration rate of braided channel
377 systems in coarse non-cohesive sediment. *Earth Surf. Process.*
378 *Landforms*, 44: 2823–2836. <https://doi.org/10.1002/esp.4710>

379 Burtin, A., Hovius, N., & Turowski, J. (2016). Seismic monitoring of torrential and
380 fluvial processes. *Earth Surface Dynamics*, 4(2), 285–307.
381 <https://doi.org/10.5194/esurf-4-285-2016>

382 Calmels, D., Galy, A., Hovius, N., Bickle, M. J., West, A. J., Chen, M.-C., Chapman,
383 H. (2011). Contribution of deep groundwater to the weathering budget in a
384 rapidly eroding mountain belt, Taiwan. *Earth and Planetary Science Letters*, 303
385 (1–2), 48–58. <https://doi.org/10.1016/j.epsl.2010.12.032>

386 Cook, K., Rekapalli, R., Dietze, M., Pilz, M., Cesca, S., Purnachandra, R., et al.
387 (2021). Early warning of catastrophic flow events using regional seismic
388 networks. *Science*, 374(6563), 87–92. <https://doi.org/10.1126/science.abj1227>

389 Dadson, S. J., Hovius, N., Chen, H., Dade, W. B., Hsieh, M.-L., Willett, S. D., Hu,
390 J.-C., Horng, M.-J., Chen, M.-C., Stark, C. P., Lague, D. Lin, J.-C. (2003). Links
391 between erosion, runoff variability and seismicity in the Taiwan orogen. *Nature*,
392 426(6967), 648–651. <https://doi.org/10.1038/nature02150>

393 Díaz, J., Gallart, J., Ruiz, M. (2014). On the Ability of the Benford's Law to Detect
394 Earthquakes and Discriminate Seismic Signals. *Seismological Research*
395 *Letters*, 86 (1), 192–201. <https://doi.org/10.1785/0220140131>

396 Dietze, M., Lagarde, S., Halfi, E., Laronne, J., & Turowski, J. (2019). Joinsensing of
397 bedload flux and water depth by seismic data inversion. *Water Resources*

398 Research, 55(11), 9892–9904. <https://doi.org/10.1029/2019WR026072>

399 Dietze, M., Hoffmann, T., Bell, R., Schrott, L., & Hovius, N. (2022). A seismic
400 approach to flood detection and characterization in upland catchments.
401 Geophysical Research Letters, 49, e2022GL100170.
402 <https://doi.org/10.1029/2022GL100170>

403 Geay, T., Belleudy, P., Gervaise, C., Habersack, H., Aigner, J., Kreisler, A., Seitz, H.,
404 and Laronne, J. B. (2017). Passive acoustic monitoring of bed load discharge in a
405 large gravel bed river. *J. Geophys. Res. Earth Surf.*, 122, 528– 545.
406 <https://doi.org/10.1002/2016JF004112>

407 Huang, J.-C., Yu, C.-K., Lee, J.-Y., Cheng, L.-W., Lee, T.-Y., and Kao,
408 S.-J. (2012). Linking typhoon tracks and spatial rainfall patterns for improving
409 flood lead time predictions over a mesoscale mountainous watershed. *Water*
410 *Resour. Res.*, 48, W09540. <https://doi:10.1029/2011WR011508>

411 Hung, C., Lin, G.-W., Kuo, H.-L., Zhang, J.-M., Chen, C.-W., Chen, H.-G. (2018).
412 Impact of an Extreme Typhoon Event on Subsequent Sediment Discharges and
413 Rainfall-Driven Landslides in Affected Mountainous Regions of Taiwan.
414 *Geofluids*, 2018. <https://doi.org/10.1155/2018/8126518>

415 Joannes-Boyau, R., Bodin, T., Scheffers, A. Sambridge, M., May, S. M. (2015). Using
416 Benford's law to investigate Natural Hazard dataset homogeneity. *Sci Rep* 5,
417 12046. <https://doi.org/10.1038/srep12046>

418 Krapesch, G., Hauer, C., and Habersack, H. (2011). Scale orientated analysis of river
419 width changes due to extreme flood hazards. *Nat.Hazards Earth Syst. Sci.*, 11,
420 2137–2147. <https://doi:10.5194/nhess-11-2137-2011>

421 Li, Q. Fu, Z., Yuan. N. (2015). Beyond Benford's Law: Distinguishing Noise from
422 Chaos. *PLoS ONE*, 10(6), e0129161. <https://doi:10.1371/journal.pone.0129161>

423 Masteller, C. C., Finnegan, N. J., Turowski, J. M., Yager, E. M., & Rickenmann, D.
424 (2019). History-dependent threshold for motion revealed by continuous bedload
425 transport measurements in a steep mountain stream. *Geophysical Research*
426 *Letters*, 46, 2583–2591. <https://doi.org/10.1029/2018GL081325>

427 Marra, F., Nikolopoulos, E. I., Creutin, J. D., & Borga, M. (2016). Space–time
428 organization of debris flows-triggering rainfall and its effect on the identification
429 of the rainfall threshold relationship. *Journal of Hydrology*, 541, 246–255.
430 <https://doi.org/10.1016/j.jhydrol.2015.10.010>

431 Nigrini, M. (1999). I've got your number: How a mathematical phenomenon can help
432 CPAS uncover fraud and other irregularities, *Journal of Accountancy*, 1-7.

433 Nigrini, M. J., Miller, S. J. (2007). Benford's Law Applied to Hydrology
434 Data—Results and Relevance to Other Geophysical Data. *Math Geol.*, 39, 469–
435 490. <https://doi.org/10.1007/s11004-007-9109-5>

436 Petley D. N., Liu C-N., Liou Y-S. (1997). Geohazards in a Neotectonic Terrain,
437 Taroko Gorge, eastern Taiwan. *Memoir of the Geological Society of China*, 40,
438 135–154.

439 Recking, A., Piton, G., Vazquez-Tarrio, D., and Parker, G. (2016). Quantifying the
440 Morphological Print of Bedload Transport. *Earth Surf. Process. Landforms*, 41,
441 809– 822. <https://doi.org/10.1002/esp.3869>.

442 Roth, D. L., Finnegan, N. J., Brodsky, E. E., Rickenmann, D., Turowski, J., Badoux,
443 A., Gimbert, F. (2017). Bed load transport and boundary roughness changes as co
444 mpeting causes of hysteresis in the relationship between river discharge and seis
445 mic amplitude recorded near a steep mountain stream. *Journal of Geophysical Re*
446 *search*, 122, 5, 1182—1200. <http://doi.org/10.1002/2016JF004062>.

447 Sambridge, M., Tkalčić, H., and Jackson, A. (2010). Benford's law in the natural

448 sciences. *Geophys. Res. Lett.*, 37, L22301. <http://doi:10.1029/2010GL044830>

449 Snyder, N. P., Castele, M. R., Wright, J. R. (2009). Bedload entrainment in
450 low-gradient paraglacial coastal rivers of Maine, U.S.A. Implications for habitat
451 restoration. *Geomorphology*, 103(3).
452 <https://doi.org/10.1016/j.geomorph.2008.07.013>

453 Stott, T., Leeks, G., Marks, S., Sawyer, A. (2001). Environmentally sensitive
454 plot-scale timber harvesting: impacts on suspended sediment, bedload and bank
455 erosion dynamics. *Journal of Environmental Management*, 63(1).
456 <https://doi.org/10.1006/jema.2001.0459>

457 Theule, J. I., Liébault, F., Loye, A., Laigle, D., and Jaboyedoff, M. (2012). Sediment
458 budget monitoring of debris-flow and bedload transport in the Manival Torrent,
459 SE France. *Nat. Hazards Earth Syst. Sci.*, 12, 731–749.
460 <https://doi.org/10.5194/nhess-12-731-2012>

461 Thorndike, R. L. (1953). Who belongs in the family?. *Psychometrika*, 18, 267–276.
462 <https://doi.org/10.1007/BF02289263>

463 Turowski, J.M., Badoux, A., Rickenmann, D. (2011), Start and end of bedload
464 transport in gravel-bed streams. *Geophysical Research Letters*, 38. <https://doi:10.1029/2010GL046558>

465

466 Turowski, J.M., Hovius, N., Meng-Long, H., Lague, D. and Men-Chiang, C. (2008),
467 distribution of erosion across bedrock channels. *Earth Surf. Process. Landforms*,
468 33: 353-363. <https://doi.org/10.1002/esp.1559>

469 Turowski, J.M., Yager, E.M., Badoux, A., Rickenmann, D. and Molnar, P. (2009). The
470 impact of exceptional events on erosion, bedload transport and channel stability
471 in a step-pool channel. *Earth Surf. Process. Landforms*, 34: 1661–
472 1673. <https://doi.org/10.1002/esp.1855>

473 Walter, F., Burtin, A., McArdell, B., Hovius, N., Weder, B., & Turowski, J. (2017).
474 Testing seismic amplitude source location for fast debris-flow detection at
475 Illgraben, Switzerland. *Natural Hazards and Earth System Sciences*, 17(6), 939–
476 955. <https://doi.org/10.5194/nhess-17-939-2017>

Figure1.

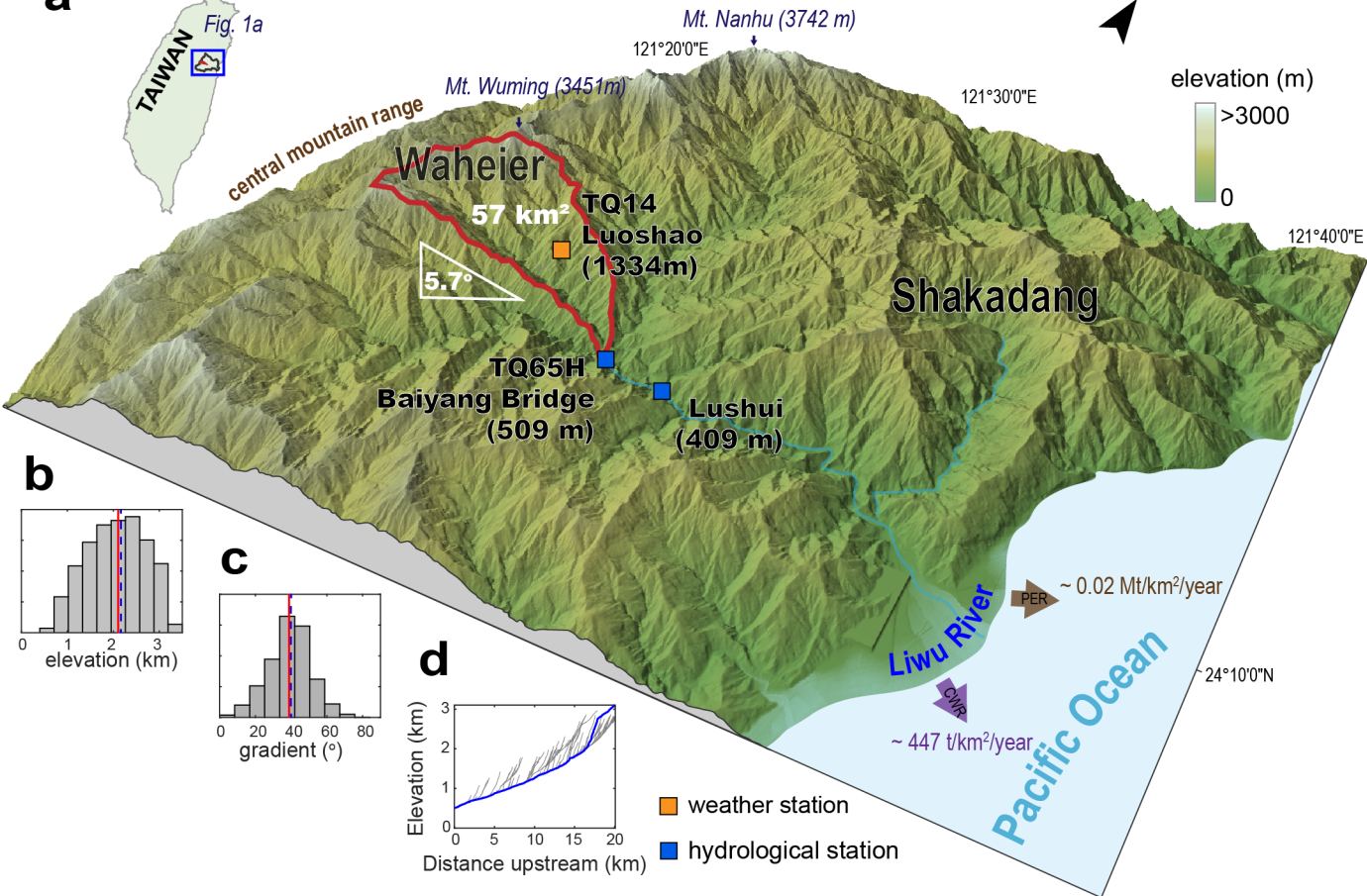
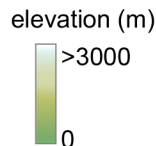
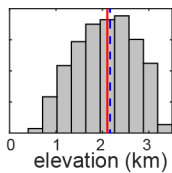
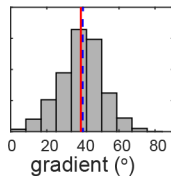
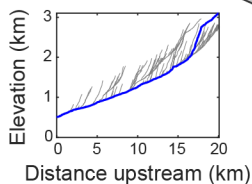
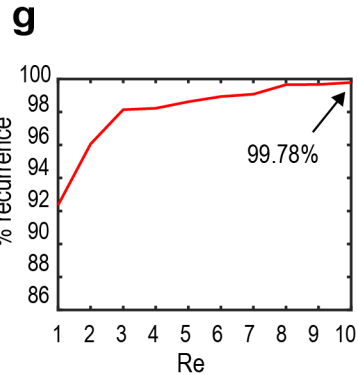
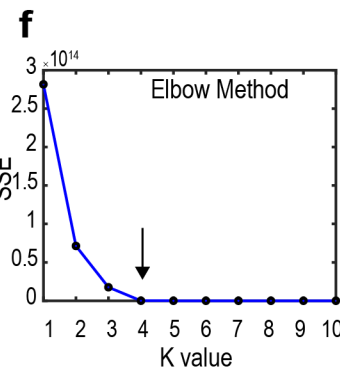
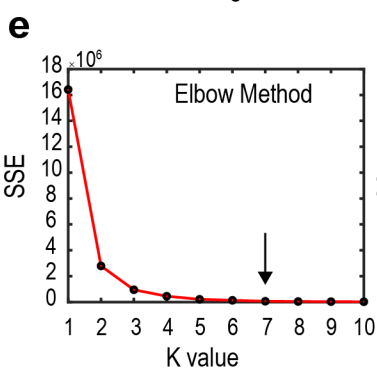
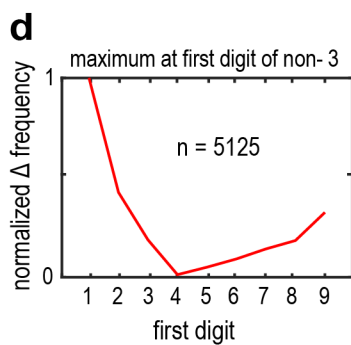
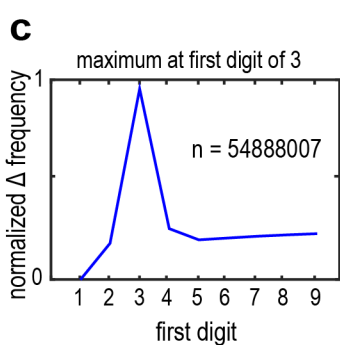
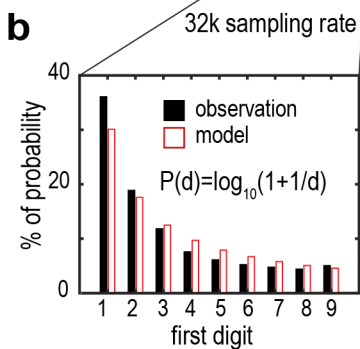
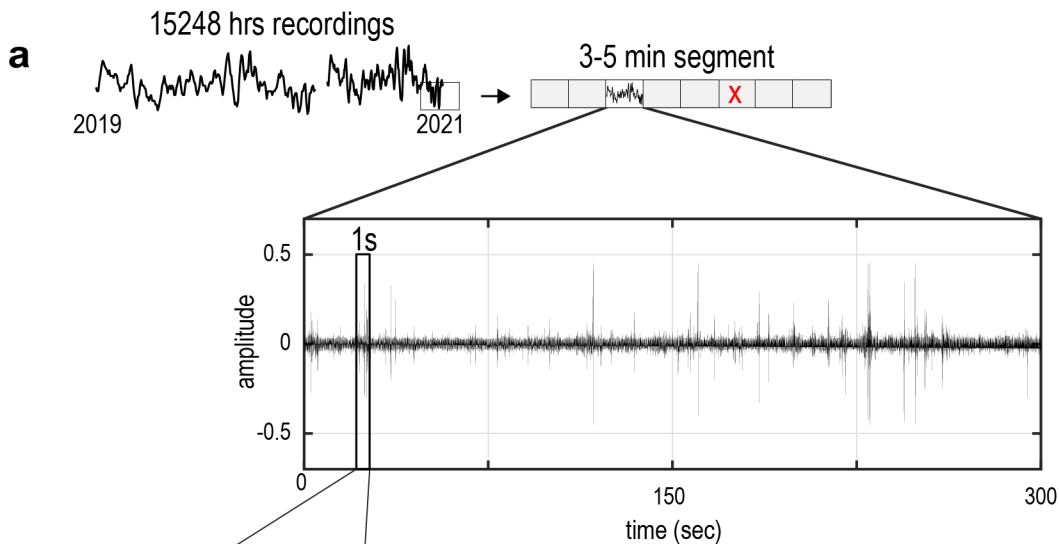
a**b****c****d**

Figure2.



h

event signals
k-means (k=7)

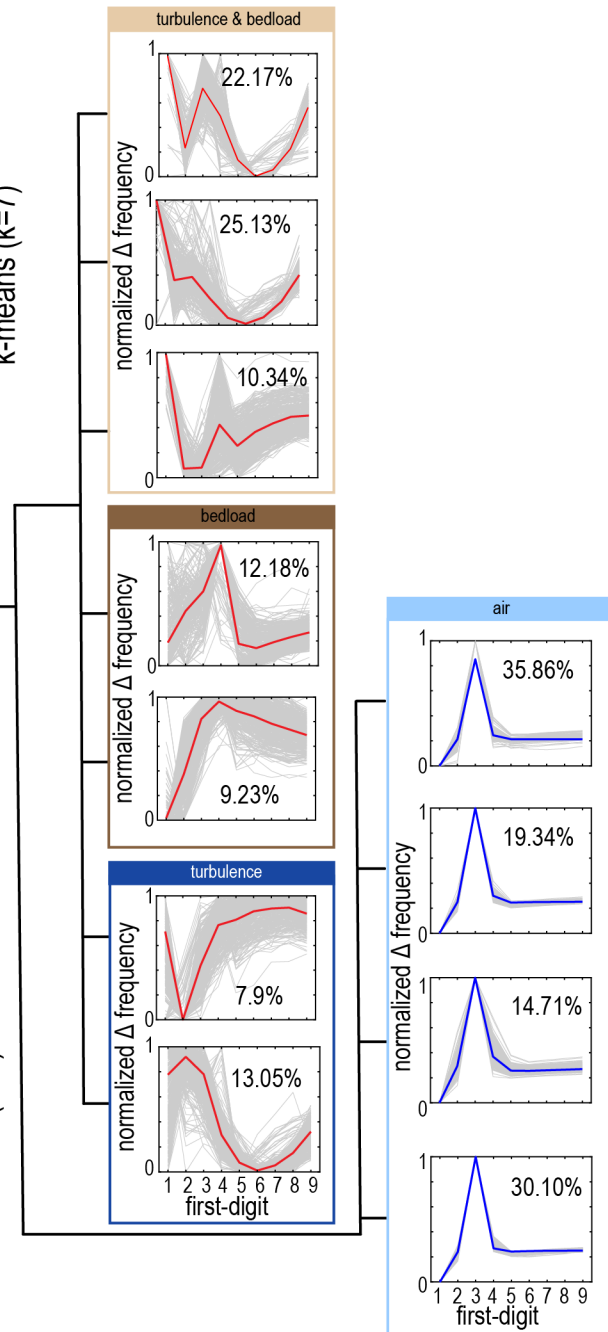


Figure3.

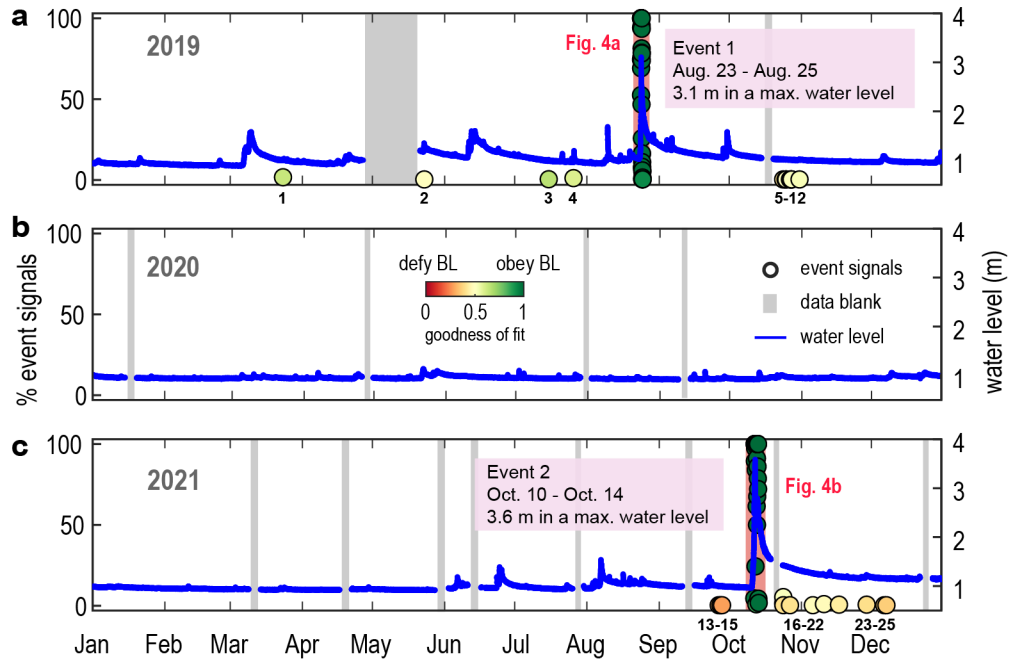


Figure4.

